

DOI:10.1002/ejic.201402957

# Biomimetic Hydroxylation Catalysis Through Self-Assembly of a Bis(pyrazolyl)methane Copper–Peroxo Complex

Claudia Wilfer,<sup>[a]</sup> Patricia Liebhäuser,<sup>[a]</sup> Hannes Erdmann,<sup>[a]</sup>  
Alexander Hoffmann,<sup>[a]</sup> and Sonja Herres-Pawlis\*<sup>[a]</sup>

**Keywords:** Bioinorganic chemistry / Oxygen activation / Self-assembly / Copper / N ligands

We synthesised and characterised four copper complexes (with copper in the oxidation states I and II) with the bis(pyrazolyl)methane ligands HC(3-*t*BuPz)<sub>2</sub>(Py) and HC(3-*t*BuPz)<sub>2</sub>(Qu). With the quinolinylligand (2-quinolinylligand)bis(3-*tert*-butylpyrazolyl)methane [HC(3-*t*BuPz)<sub>2</sub>(Qu)] we obtained the tetrahedral monofacial complex [CuCl{HC(3-*t*BuPz)<sub>2</sub>(Qu)}] (**C1**) and with the pyridinyl ligand (2-pyridinyl)bis(3-*tert*-butylpyrazolyl)methane [HC(3-*t*BuPz)<sub>2</sub>(Py)] we obtained the three complexes [CuCl{HC(3-*t*BuPz)<sub>2</sub>(Py)}] (**C2**), [CuBr<sub>2</sub>{HC(3-*t*BuPz)<sub>2</sub>(Py)}] (**C3**) and [CuCl<sub>2</sub>{HC(3-*t*BuPz)<sub>2</sub>(Py)}] (**C4**), which are also monofacially coordinated. The mo-

lecular structures were analysed and compared with density functional theory calculations, which included natural bond orbital (NBO) analysis. **C1** can, when generated in situ, serve as part of a precursor, used for the activation of oxygen as tyrosinase model. We observe the self-assembly of a peroxo-dicopper complex **P** with the HC(3-*t*BuPz)<sub>2</sub>(Qu) ligand, which is able to perform catalytic hydroxylation catalysis with phenols. DFT calculations were also carried out to understand the electronic transitions responsible for the UV/Vis bands in the corresponding spectra of the peroxo species.

## Introduction

Bis(pyrazolyl)methane ligands represent a group of versatile heteroscorpionate ligands<sup>[1]</sup> that play an increasingly important and promising role in the investigation of tyrosinase models.<sup>[2,3]</sup> Several changes throughout the years concerning substituents and steric properties of the substituents led to the so-called second generation of bis(pyrazolyl)methane ligands, which refers to the fact that these ligands carry substituents (e.g., alkyl groups) at their pyrazolyl moieties and therefore enforce a monofacial coordination mode.<sup>[4]</sup> The most common donors, besides the two pyrazolyl substituents, are pyridinyl, imidazolyl and quinolinylligand as they represent aromatic nitrogen donors that in part resemble the biological surrounding of metal atoms in the active centre of enzymes (e.g., histidine).<sup>[5]</sup>

Tyrosinase is a widespread type III copper enzyme that catalyses the *ortho*-hydroxylation of monophenols and the subsequent oxidation of the resulting catechols to *o*-quinones.<sup>[5–8]</sup> Tyrosinase therefore has monophenolase and diphenolase activity.<sup>[5,9]</sup> The first step in the reaction cycle is the activation of dioxygen, which results in a (μ-η<sup>2</sup>:η<sup>2</sup>)-dicopper(II) peroxide core.<sup>[5,6,10]</sup> These species can be char-

acterised well by using UV/Vis spectroscopy owing to their significant UV/Vis bands and their characteristic intensity ratio.<sup>[10,11]</sup> Experimental evidence for the unique O<sub>2</sub> binding mode in the structurally related oxy-hemocyanin was previously obtained from the structural characterisation of a Cu/O<sub>2</sub> model species by Kitajima et al. in 1989.<sup>[12–14]</sup> Finally, in 2006, Matoba et al. were able to present the first crystal structure of tyrosinase, which also proved that histidine residues surround the copper atoms in the active site.<sup>[8]</sup> Tyrosinase catalyses the reaction of melanin from tyrosine. Melanin itself is a brown pigment that is widespread in mammals, birds and plants.<sup>[15–18]</sup>

A multitude of ligand families such as tris(pyrazolyl)borates,<sup>[12]</sup> tris(pyrazolyl)methanes,<sup>[19]</sup> alkylamines,<sup>[20]</sup> pyridines,<sup>[21]</sup> ketimines<sup>[22]</sup> and guanidines<sup>[23,24]</sup> have been investigated as building blocks of hemocyanine and tyrosinase models in recent years. When treating Cu<sup>I</sup> species with O<sub>2</sub>, there are two major products that can be generated: the (μ-η<sup>2</sup>:η<sup>2</sup>)-peroxide core (**S**P core) and the bis(μ-oxo)dicopper(III) core (**O** core), which are nearly isoenergetic and exist in equilibrium at low temperatures.<sup>[11,25,26]</sup> However it was discovered that whether the **S**P or the **O** core is preferably generated depends on the steric properties and mostly on the basicity of the ligands used. A hybrid permethylated amine–guanidine ligand, for example, only forms the **O** core, which suggests that bidentate sterically nondemanding strong σ donors shift the equilibrium toward the Cu<sup>III</sup> **O** complex.<sup>[11,27,28]</sup> After reaction with the **O** and **P** complex, sometimes bis(μ-hydroxo)dicopper(II)

[a] Department of Chemistry, Ludwig-Maximilians-Universität München, Butenandtstraße 5–13, 81377 München, Germany  
E-mail: sonja.herres-pawlis@cup.uni-muenchen.de  
<http://www.cup.lmu.de/ac/herres-pawlis/>

Supporting information for this article is available on the WWW under <http://dx.doi.org/10.1002/ejic.201402957>.

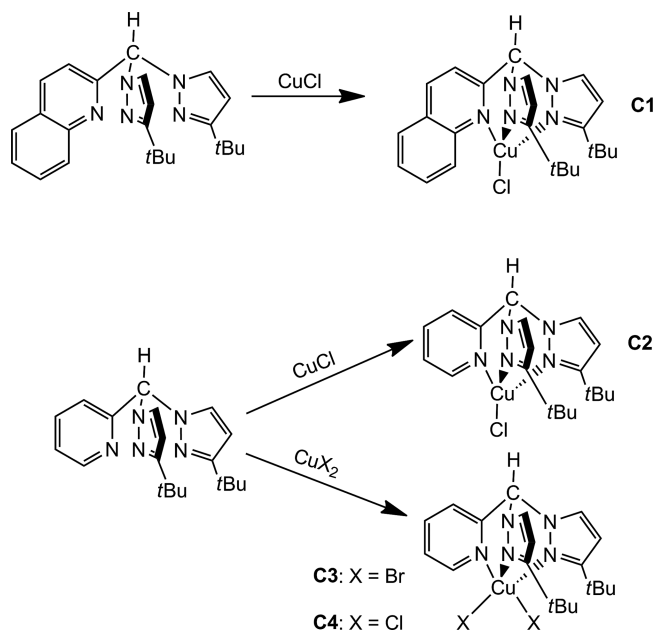
complexes can be isolated as products of hydrolysis.<sup>[29]</sup> In the  $\text{Cu}_2\text{O}_2$  model chemistry a large variety of further  $\text{Cu}_2\text{O}_2$  species have been observed, but for tyrosinase activity, **O** and **P** cores are mainly discussed.<sup>[5,7]</sup>

When investigating enzyme models, it is clear that an extremely important part of the work, in addition to the imitation of the active site, lies in the testing of the catalytic abilities of the model. With regard to the reaction mechanism of tyrosinase, in 2009 Casella et al. proved that during substrate transformation of *Streptomyces antibioticus* tyrosinase, the  $(\mu\text{-}\eta^2\text{:}\eta^2)$ -peroxide core remained the only enzyme species present.<sup>[30]</sup> Until now only three systems achieved significant catalytic phenol hydroxylation using dioxygen. The first one was discovered by Réglie et al.,<sup>[31]</sup> the second one by Tuzek et al.<sup>[32]</sup> and the third one by Herres-Pawlis et al.<sup>[2]</sup> Tuzek et al. recently published another related catalytic system that uses ligands that consist of imine and benzimidazole and imine and pyrazole moieties, respectively.<sup>[33,34]</sup> Very recently, Lumb et al. made use of catalytic copper–dioxygen chemistry to generate valuable organic products out of simple substituted phenols.<sup>[35,36]</sup> This indicates the general importance of bioinorganic copper chemistry as a synthetic tool. It has to be noted that the peroxide species is constructed by means of self-assembly, which means that when all components are mixed, the ordered peroxide builds itself without influence from the outside. However, different possibilities of “self-assembly” exist. For instance, Stack et al. showed that the peroxide core is formed by mixing imidazole ligands, copper salts and dioxygen, but the phenolate had to be added afterwards for hydroxylation reactivity.<sup>[10]</sup> Tuzek et al. observed the self-assembly with catalytic activity for tyrosinase models with pyridine–imine ligands by mixing copper phenolates, ligands and dioxygen.<sup>[32]</sup> The role of the stabilising ligands is crucial for the formation and reactivity of the species. We recently explored how different donor properties influence the coordination chemistry and complex structure of different transition-metal bis(pyrazolyl)methane complexes.<sup>[37]</sup>

Here we report four new bis(pyrazolyl)methane–copper complexes with the  $\text{HC}(3\text{-}t\text{BuPz})_2(\text{Py})$  and  $\text{HC}(3\text{-}t\text{BuPz})_2(\text{Qu})$  ligands. We have investigated the structure of these complexes and analysed their donor situation by means of density functional theory calculations. We studied the donor rivalry between pyridinyl/quinolinyl and pyrazolyl nitrogen atoms by comparing their charge-transfer energies. Moreover, the formation of the peroxo species  $[\text{Cu}_2\text{O}_2\{\text{HC}(3\text{-}t\text{BuPz})_2(\text{Qu})\}]_2[\text{SbF}_6]_2$  was monitored by means of UV/Vis spectroscopy. By using the self-assembly approach, we observed catalytic activity in the *ortho*-hydroxylation of the substrate *para*-methoxyphenol and subsequent oxidation to quinones when using the new  $[\text{Cu}_2\text{O}_2\{\text{HC}(3\text{-}t\text{BuPz})_2(\text{Qu})\}]_2[\text{SbF}_6]_2$  system. Finally, natural bond orbital (NBO) and natural transition orbital (NTO) calculations were carried out for the peroxo complex to understand the bonding situation in this species, and furthermore to gain insight into the electron transitions that generate the UV/Vis bands.

## Results and Discussion

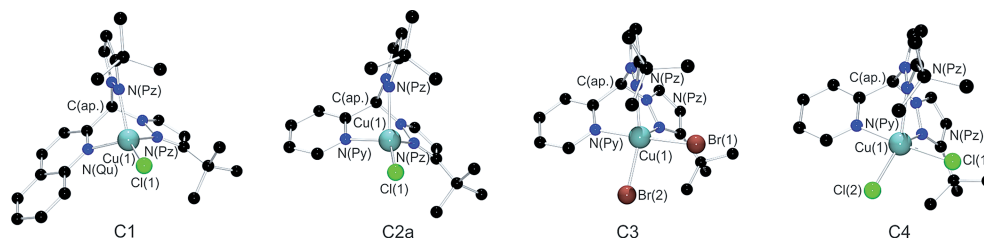
The reaction of the ligands  $\text{HC}(3\text{-}t\text{BuPz})_2(\text{Qu})$  and  $\text{HC}(3\text{-}t\text{BuPz})_2(\text{Py})$  with various copper salts led to the formation of four complexes (**C1**–**C4**; Scheme 1). Single crystals for X-ray crystallography were obtained by cooling the reaction solutions to 5 °C for a couple of days or by simply storing the solution in a vibration-free environment at room temperature (see the Experimental Section for details). With the ligand  $\text{HC}(3\text{-}t\text{BuPz})_2(\text{Qu})$  we isolated  $[\text{CuCl}\{\text{HC}(3\text{-}t\text{BuPz})_2(\text{Qu})\}]$  (**C1**); with the ligand  $\text{HC}(3\text{-}t\text{BuPz})_2(\text{Py})$  we isolated  $[\text{CuCl}\{\text{HC}(3\text{-}t\text{BuPz})_2(\text{Py})\}]$  (**C2**),  $[\text{CuBr}_2\{\text{HC}(3\text{-}t\text{BuPz})_2(\text{Py})\}]$  (**C3**) and  $[\text{CuCl}_2\{\text{HC}(3\text{-}t\text{BuPz})_2(\text{Py})\}]$  (**C4**). All four complexes are coordinated by only one heteroscorpionate ligand owing to steric shielding of alkyl groups in the 3-position of the pyrazolyl units (Figure 1).<sup>[1,4]</sup> Selected bond lengths and bond angles are shown in Table 1, which also includes the  $\tau$  value, which provides an easy determination of the coordination mode around the metal centre.<sup>[38,39]</sup> All relevant crystallographic data are collected in Table 4. Complex **C2** appears in the solid state in two slightly differing conformers, dubbed **C2a** and **C2b**, whereas in **C3** both molecules of the asymmetric unit exhibit the same conformer (see Table S1 in the Supporting Information).



Scheme 1. Synthesis of **C1**–**C4**.

In **C1** and **C2** the metal ion is four-coordinate. The nitrogen donors of the bis(pyrazolyl)methane ligand occupy three coordination sites; the remaining one is occupied by one halogenido ligand, thereby resulting in an overall distorted-tetrahedral geometry (Figure 1) with nearly identical  $\tau_4$  values.

Bond angles deviate more from the ideal tetrahedral angle for **C1**. In both complexes **C1** and **C2b**  $\text{Cu-N}_{\text{Pz}}$  bond lengths are shorter than the corresponding  $\text{Cu-N}_{\text{Py}}$  or  $\text{Cu-N}_{\text{Qu}}$  bond lengths, which is in contrast to **C2a**, **C3** and **C4**.

Figure 1. Molecular structures of **C1**–**C4**.Table 1. Selected bond lengths [Å] and angles [°] of **C1**–**C4**.

	<b>C1</b> <sup>[a]</sup>	<b>C2a</b> <sup>[a]</sup>	<b>C2b</b> <sup>[a]</sup>	<b>C3</b> <sup>[b]</sup>	<b>C4</b> <sup>[a]</sup>
Cu–N <sub>Pz</sub>	2.124(2)	2.106(2)	2.082(2)	2.117(6)	2.233(3)
Cu–N <sub>Py</sub> /Cu–N <sub>Qu</sub> *	2.149(2)*	2.183(2)	2.120(2)	2.421(6)	2.058(4)
Cu–X	2.215(1)	2.120(2)	2.132(2)	2.388(1)	2.225(2)
C <sub>apical</sub> –N <sub>Pz</sub>	1.456(2)	2.199(1)	2.187(1)	2.409(1)	2.267(1)
C <sub>apical</sub> –C <sub>Py</sub> /C <sub>apical</sub> –C <sub>Qu</sub> *	1.511(4)*	1.449(3)	1.450(3)	1.441(9)	1.448(3)
N <sub>Pz</sub> –Cu–X(1)	124.2(1)	1.449(3)	1.460(3)	1.458(9)	1.515(6)
N <sub>Pz</sub> –Cu–X(2)	124.2(1)	1.519(4)	1.507(3)	1.503(10)	1.515(6)
N <sub>Py</sub> –Cu–X(1)/N <sub>Qu</sub> –Cu–X(1)*	–	130.0(1)	130.9(1)	115.2(2)	133.6(1)
N <sub>Py</sub> –Cu–X(2)/N <sub>Qu</sub> –Cu–X(2)*	–	127.2(1)	129.3(1)	151.7(2)	133.6(1)
N <sub>Pz</sub> –Cu–N <sub>Pz</sub>	–	–	–	93.5(2)	93.5(2)
N <sub>Pz</sub> –Cu–N <sub>Py</sub> /N <sub>Pz</sub> –Cu–N <sub>Qu</sub> *	89.1(1)	90.5(1)	86.6(1)	95.2(2)	93.5(1)
X(1)–Cu–X(2)	–	88.5(1)	90.8(1)	92.2(2)	93.3(1)
τ <sub>4</sub> <sup>[c]</sup> , τ <sub>5</sub> <sup>[d]</sup>	0.76	86.0(1)	88.7(1)	176.6(2)	175.9(1)
		–	–	90.6(1)	90.8(1)
		0.73	0.71	0.42*	0.71*

$$[a] X = \text{Cl}. [b] X = \text{Br}. [c] \tau_4 = \frac{360^\circ - (a + \beta)}{141}. [d] \tau_5 = \frac{(\beta - a)}{60}.$$

In general, bis(pyrazolyl)methane complexes show a donor competition between their N donors, which appears here again.<sup>[37,40]</sup> This effect is discussed in more detail in the next paragraph.

In **C3** and **C4** the metal ion is five-coordinate. The nitrogen donors of the bis(pyrazolyl)methane ligand occupy three coordination sites; the other two are occupied by halogenido ligands, thereby resulting in an overall distorted square-pyramidal geometry for **C3** and a distorted trigonal-bipyramidal one for **C4** (Figure 1). In both **C3** and **C4**, Cu–N<sub>Py</sub> bond lengths are shorter than the corresponding Cu–N<sub>Pz</sub> ones. It is difficult to determine which nitrogen is the stronger donor, as basicity and nucleophilicity have to be taken into account. Normally the donor competition is won by pyrazolyl (see **C1** and **C2b** with distorted-tetrahedral environments),<sup>[37]</sup> but in **C3** and **C4** with fivefold coordination it is the other way round. The sterically demanding *tert*-butyl groups might hinder the pyrazolyl unit from coming closer to the metal ion. The Cu–Cl bond length in **C4** is naturally shorter than the Cu–Br bond length in **C3**, which is in agreement with common Cu–X bond lengths. The N<sub>Pz</sub>–Cu–Cl(1)/N<sub>Pz</sub>–Cu–Br(1) and N<sub>Pz</sub>–Cu–Cl(2)/N<sub>Pz</sub>–Cu–Br(2) bond angles reflect (as already suggested by the τ values) that **C3** is distorted and cannot really be assigned to a specific geometry and that **C4** is of distorted trigonal-bipyramidal geometry. For **C4** the pyridinyl N donor and

Cl(2) reside at the axial positions, whereas the two pyrazolyl N donors and Cl(1) form the equatorial positions. C<sub>apical</sub>–N<sub>Pz</sub> bond lengths are the same for **C3** and **C4**.

We performed density functional theory calculations to analyse the coordination of all four complexes. The TPSSh functional in combination with the double-ζ basis set 6-31G(d) was used, since this combination yielded good results in the benchmarking of Cu<sub>2</sub>O<sub>2</sub> complexes.<sup>[3]</sup> Key geometric parameters of the theoretical calculations of **C1**–**C4** are listed in Table 2. These data show that another conformer was found for **C2**, which is reflected by the significantly smaller N<sub>Qu</sub>–Cu–Cl angle, so that these data are not discussed in this section. All attempts to find the other conformer failed. However, the experimental structure of **C1** is in good agreement with the theoretical values for bond lengths and angles. Only the predicted Cu–N<sub>Qu</sub> bond length is a bit too short. The N<sub>Pz</sub>–Cu–N<sub>Pz</sub> and N<sub>Qu</sub>–Cu–N<sub>Pz</sub> angles are predicted to be about 4° too large. Moreover the N<sub>Qu</sub>–Cu–Cl(1) bond angle is predicted to be too small, but the N<sub>Pz</sub>–Cu–Cl(1) angle is in good agreement with the experimental data.

For the five-coordinate complexes **C3** and **C4** it can be seen that the theoretical data are in accord with the experimental data as well. In complex **C3** all relevant bond lengths are predicted well. The mirror plane in **C4** is also found for the ground-state calculation. In **C4**, with the ex-

Table 2. Key bond lengths [ $\text{\AA}$ ] and angles [ $^\circ$ ] of **C1**–**C4** [Gaussian 09, TPSSh/6-31G(d)].<sup>[41]</sup>

	<b>C1</b> <sup>[a]</sup>	<b>C2</b> <sup>[a]</sup>	<b>C3</b> <sup>[b]</sup>	<b>C4</b> <sup>[a]</sup>
Cu–N <sub>Pz</sub>	2.011	1.982	2.071 2.397	2.161
Cu–N <sub>Py</sub> /Cu–N <sub>Qu</sub> *	1.975	2.009	2.056	2.060
Cu–X	2.262	2.243	2.342 2.352	2.274 2.264
C <sub>apical</sub> –N <sub>Pz</sub>	1.458	1.460	1.459 1.449	1.453
C <sub>apical</sub> –C <sub>Py</sub> /C <sub>apical</sub> –C <sub>Qu</sub> *	1.522	1.524	1.521	1.520
N <sub>Pz</sub> –Cu–X(1)	122.7	130.0	121.6 138.9	130.2
N <sub>Pz</sub> –Cu–X(2)	–	–	87.4 90.7	90.4
N <sub>Py</sub> –Cu–X(1)/N <sub>Qu</sub> –Cu–X(1)*	122.4	106.3	163.2	168.6
N <sub>Py</sub> –Cu–X(2)/N <sub>Qu</sub> –Cu–X(2)*	–	–	95.8	93.0
N <sub>Pz</sub> –Cu–N <sub>Pz</sub>	93.7	94.1	98.6	98.2
N <sub>Pz</sub> –Cu–N <sub>Py</sub> /N <sub>Pz</sub> –Cu–N <sub>Qu</sub> *	93.8	92.2	77.7 84.0	82.1
X(1)–Cu–X(2)	–	–	98.6	98.4
$\tau_4$ , <sup>[39]</sup> $\tau_5$ * <sup>[38]</sup>	0.81	0.88	0.41*	0.64*

$$[\text{a}] \text{ X} = \text{Cl.} [\text{b}] \text{ X} = \text{Br.} [\text{c}] \tau_4 = \frac{360^\circ - (a + \beta)}{141}. [\text{d}] \tau_5 = \frac{(\beta - a)}{60}.$$

ception of the Cu–N<sub>Pz</sub> bond length, which is predicted to be too short, all other bond lengths conform to the experimental data. Looking at the bond angles in complexes **C3** and **C4**, it is noteworthy that the N<sub>Pz</sub>–Cu–Cl(1) and N<sub>Pz</sub>–Cu–Cl(2) angles in **C4** are predicted quite well, whereas the corresponding angles in **C3** are predicted to be either too large or too small. With the exception of the N<sub>Py</sub>–Cu–Cl(2) angle, which is predicted to be too small, the remaining bond angles are predicted to be 3–8° too large with the one other exception of the N<sub>Pz</sub>–Cu–N<sub>Py</sub> angle in **C3**. As for  $\tau$  values, the predicted and experimental ones coincide well. For **C3** the experimental and calculated  $\tau$  values match almost exactly. For **C2** a comparison would not make sense, as different conformers were found. The geometry of **C1** is predicted to be a bit more distorted tetrahedral than observed experimentally. For **C4** the calculated  $\tau_5$  value identifies a slightly less distorted trigonal-bipyramidal geometry than the experimental data suggests.

In addition to DFT calculations, NBO analyses were performed of the optimised structures of **C1**–**C4** (Table 3).<sup>[42–44]</sup> The second-order perturbation theory yields the charge-transfer energies for the donation from the pyrazolyl or pyridinyl units to copper.

Table 3. Charge-transfer energies [kcal mol<sup>−1</sup>] for **C1**–**C4** and **P** [Gaussian 09, TPSSh/6-31G(d) and NBO 6.0].

	<b>C1</b>	<b>C2a</b> <sup>[a]</sup>	<b>C3</b>	<b>C4</b>	<b>P</b>
CT energies					
N <sub>Pz</sub> →M	32.4	29.7	17.9	14.4	39.2
N <sub>Py</sub> →M	32.4	27.0	8.5	14.4	32.2
N <sub>Py</sub> /N <sub>Qu</sub> *→M	32.5*	24.2	18.4	17.4	17.2*

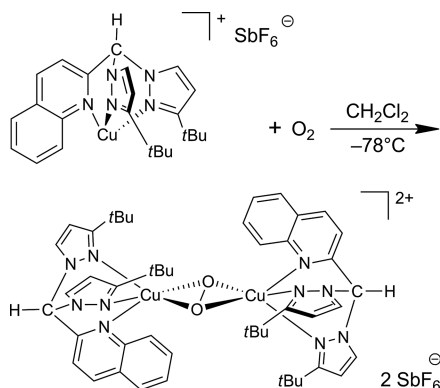
[a] Data obtained directly from crystal structure (not optimised).

At a glance it can be seen that the charge-transfer energies mostly correlate with the M–N bond lengths. In gene-

ral, the larger the charge-transfer energy is, the shorter is the respective M–N bond. Both four-coordinate complexes **C1** and **C2** show similar charge-transfer energy values. Additionally, in **C1** the bond lengths for the Cu–N<sub>Pz</sub> and Cu–N<sub>Qu</sub> bonds are similar, which is also reflected in the similar values for the charge-transfer energies. Different charge-transfer energies for the N<sub>Pz</sub>–M bond are represented by different N<sub>Pz</sub>–M bond lengths. In **C2a** the charge-transfer energy of pyridinyl to copper is smaller than the respective energy for pyrazolyl. This does not correlate with the medium-long Cu–N<sub>Py</sub> bond. A better correlation is found in **C3** and **C4**. Charge-transfer energies for N<sub>Pz</sub>–Cu are different in **C3**, which is in accord with different Cu–N<sub>Pz</sub> bond lengths. The donor ability is predicted to be slightly higher for pyridinyl, therefore the Cu–N<sub>Py</sub> bond length should be shorter than the Cu–N<sub>Pz</sub> bond length, as found experimentally. In **C4** the charge-transfer energies are exactly the same for both pyrazolyl–M interactions. Theoretical calculations showed equal Cu–N<sub>Pz</sub> bond lengths owing to the mirror plane in **C4**, so the values for the charge-transfer energy tie in with that. Moreover the charge-transfer energy for pyridinyl is slightly larger than that for the pyrazolyl, which again is reflected in the shorter Cu–N<sub>Py</sub> bond length. To summarise, our NBO analysis shows that for the five-coordinate complexes the pyridinyl units donate slightly more than the pyrazolyl units. The opposite applies to **C2a**. Here the donor rivalry between pyrazolyl and pyridinyl/quinolinyl that has been observed before can be seen clearly.<sup>[37]</sup>

In addition to structural determinations, the bis(pyrazolyl)methane complex **C1** was used as a precursor in the activation of oxygen. As described in the introduction, bis-(pyrazolyl)methane ligands can be used as promising building blocks for tyrosinase models for the activation of oxygen. However, owing to its insolubility, **C1** could not be used directly but had to be generated in situ from the starting compounds following the synthetic route described by Herres-Pawlis et al.<sup>[2]</sup> The resulting species was hence treated with AgSbF<sub>6</sub> immediately and the precursor [Cu{HC(3-*t*BuPz)<sub>2</sub>(Qu)}][SbF<sub>6</sub>] could be obtained. This precursor was then injected into an O<sub>2</sub>-saturated CH<sub>2</sub>Cl<sub>2</sub> solution at 195 K (see Scheme 2). The formation of the resulting peroxo complex [Cu<sub>2</sub>O<sub>2</sub>{HC(3-*t*BuPz)<sub>2</sub>(Qu)}<sub>2</sub>][SbF<sub>6</sub>]<sub>2</sub> (**P**[SbF<sub>6</sub>]<sub>2</sub>) was monitored by means of UV/Vis spectroscopy (Figure 2). The spectrum shows a band at 345 nm and an almost unidentifiable one at 550 nm. These two bands stem from ligand-to-metal charge-transfer (LMCT) transitions. They are in good analogy with the UV/Vis bands found for oxy-tyrosinase and oxy-hemocyanin.<sup>[45]</sup> Additional bands in the area of 305–320 nm originate from intraligand transitions. It could be noticed that the reaction is very slow, so that the peroxo species was only formed in 80% yield after 8 h (Figure 2). Longer reaction times led to the decay of **P**[SbF<sub>6</sub>]<sub>2</sub>. This excluded Raman or X-ray absorption spectroscopy (XAS) studies. This is in contrast to the parent **P** species [Cu<sub>2</sub>O<sub>2</sub>{HC(3-*t*BuPz)<sub>2</sub>(Py)}<sub>2</sub>][SbF<sub>6</sub>]<sub>2</sub>, which is formed within seconds and stable for days at −78 °C.<sup>[2]</sup> Further analyses involved the

determination of the kinetics for the formation of the peroxo compound. It could be shown that for the first 250 min the reaction follows pseudo-first-order kinetics with a reaction rate of  $k = 5.4 \times 10^{-3} \text{ s}^{-1}$  (see Figure S1 in the Supporting Information). After formation, the **P** core decays at  $-78^\circ\text{C}$  with  $t_{1/2}$  of 1.46 min at  $0^\circ\text{C}$  (Figure S2).



Scheme 2. Formation of  $[\text{Cu}_2\text{O}_2\{\text{HC}(3\text{-}t\text{BuPz})_2(\text{Qu})\}_2][\text{SbF}_6]_2$  (**P** $[\text{SbF}_6]_2$ ).

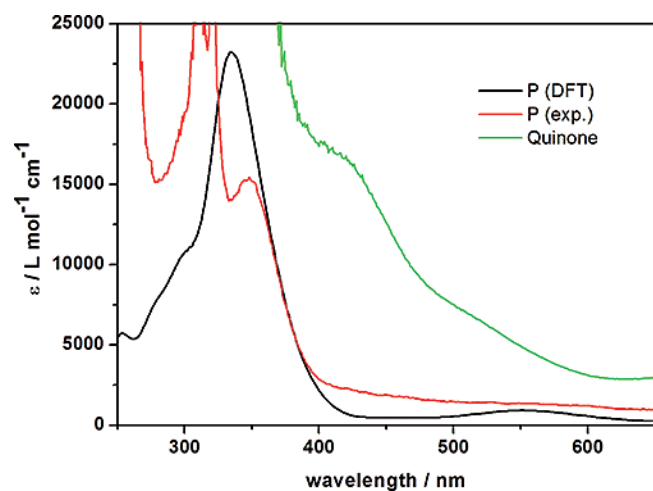


Figure 2. UV/Vis spectrum of  $[\text{Cu}_2\text{O}_2\{\text{HC}(3\text{-}t\text{BuPz})_2(\text{Qu})\}_2][\text{SbF}_6]_2$  (**P** $[\text{SbF}_6]_2$ ) (experimental in red and theoretical in black) and the final UV/Vis spectrum of the formation of the quinone in the self-assembly mode (green).

NTO analysis<sup>[46]</sup> of the UV/Vis transitions (Figure 3) obtained by time-dependent DFT [TPSSH/6-31G(d)] reveals that the visible transition at 550 nm is the classical out-of-plane  $\pi_v^* \rightarrow d_{xy}$  LMCT. The accepting orbital is called the lowest unoccupied NTO (LUNTO). With regard to symmetry and composition it is in accord with the classical  $\text{Cu}_2\text{O}_2$  theory.<sup>[6]</sup> The broad shoulder stems from a transition from pyrazolyl  $\pi$ - and quinolinylyl  $\sigma$ -donating orbitals into the same LUNTO. This is in accord with the NTO analysis performed for the original pyridinyl peroxo system.<sup>[2]</sup> The UV transitions all have mixed character; they are transitions between the in-plane  $\pi_{\sigma^*}$  orbital and the ligands into the  $d_{xy}$  copper orbital. It is highly remarkable that in **P**, the

pyrazolyl units donate more strongly to copper than the quinolinylyl units (Table 3), which underlines the complicated donor situation at  $\text{Cu}^{\text{II}}$  in comparison to **C3** and **C4** once more.

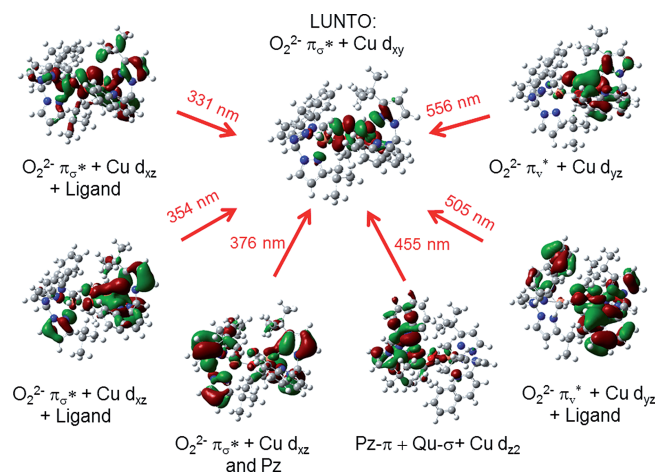


Figure 3. NTO analysis of  $[\text{Cu}_2\text{O}_2\{\text{HC}(3\text{-}t\text{BuPz})_2(\text{Qu})\}_2]^{2+}$  (**P**).

Despite the low stability of the **P** species, we observed an astonishing hydroxylation reactivity of this species when all components were combined in a self-assembly reaction [i.e., copper(I) precursor, 4-methoxyphenol (25 equiv.) and triethylamine (50 equiv.) and subsequent addition of oxygen following the protocol of Tucek et al.<sup>[32]</sup> The hydroxylation and subsequent oxidation yielded the biomimetic quinone product, which can be observed by UV/Vis spectroscopy owing to its intense absorption at 418 nm (see Figure 2). Hereby, a turnover number of 10 in 1 h could be monitored. This shows that the **P** species formed as a reactive intermediate during oxygenation. The direct capture of the **P** species at room temperature was not possible. However, the formation of **P** $[\text{SbF}_6]_2$  and phenol hydroxylation is fast enough to compete with the decay and we assume the same mechanism here as for the parent **P** species  $[\text{Cu}_2\text{O}_2\{\text{HC}(3\text{-}t\text{BuPz})_2(\text{Py})\}_2][\text{SbF}_6]_2$ . The NBO donor study on **P** and the related complexes indicates that the interplay between pyridinyl and pyrazolyl units explains the hydroxylation chemistry; the pyrazolyl appears to donate more strongly (Table 3) but the smaller steric requirements of the pyridinyl allows the approach of substrates. This result shows that bis(pyrazolyl)pyridinylmethane copper complexes possess a large potential for further catalytic hydroxylation applications in synthetic organic chemistry.

## Conclusion

Herein we have presented four bis(pyrazolyl)pyridinylmethane copper complexes (with copper in the oxidation states I and II) with the bis(pyrazolyl)methane ligands  $\text{HC}(3\text{-}t\text{BuPz})_2(\text{Py})$  and  $\text{HC}(3\text{-}t\text{BuPz})_2(\text{Qu})$ . With the quinolinylyl ligand  $\text{HC}(3\text{-}t\text{BuPz})_2(\text{Qu})$  we obtained the tetrahedral monofacial complex  $[\text{CuCl}\{\text{HC}(3\text{-}t\text{BuPz})_2(\text{Qu})\}]$

(C1) and with the pyridinyl ligand HC(3-*t*BuPz)<sub>2</sub>(Py) we obtained the tetrahedral complex [CuCl{HC(3-*t*BuPz)<sub>2</sub>(Py)}] (C2), the distorted square-pyramidal complex [CuBr<sub>2</sub>{HC(3-*t*BuPz)<sub>2</sub>(Py)}] (C3) and the distorted trigonal-bipyramidal complex [CuCl<sub>2</sub>{HC(3-*t*BuPz)<sub>2</sub>(Py)}] (C4). The donor situation was studied by NBO analysis but a mixed picture was found. Depending on the coordinative situation both pyrazolyl and pyridinyl units can win the competition. C1 can – when generated in situ – serve as part of a precursor that can be used for the activation of oxygen as tyrosinase models. We observed the self-assembly of a peroxo–dicopper complex with the HC(3-*t*BuPz)<sub>2</sub>(Qu) ligand, which is able to perform catalytic hydroxylation catalysis with phenols. The observed coordinative flexibility of the bis(pyrazolyl)pyridinylmethane ligands might be important for the functionality of the generated P species.

## Experimental Section

**General:** All experiments that involved moisture- and air-sensitive compounds were carried out by using standard Schlenk techniques. All chemicals were purchased from Fluka or ABCR and were used as received without further purification. The solvents used were dried by standard literature procedures.<sup>[47]</sup> The ligands HC(3-*t*BuPz)<sub>2</sub>(Py) and HC(3-*t*BuPz)<sub>2</sub>(Qu) were synthesised according to the literature, as was CuCl.<sup>[48,49]</sup>

**Physical Methods:** Fast-atom bombardment (FAB) mass spectra were obtained with a Thermo Finnigan MAT 95 mass spectrometer for C1–C3, whereas mass spectra for C4 were recorded with a Thermoquest Finnigan spectrometer in the ESI-MS mode (70 eV). Infrared spectra were recorded with a Jasco FTIR 460 spectrophotometer in the range of 650–3500 cm<sup>-1</sup>. UV/Vis spectra were recorded with a Varian Cary 60 spectrophotometer. Elemental analyses were performed with a Vario EL or Vario MICRO CHNS Analyser.

**X-ray Analyses:** The crystal data for C1–C4 are presented in Table 4. The data for C1 was collected with a KappaCCD (Bruker AXS BV), for C2 with a D8 Quest and for C3 with a Bruker D8 Quest diffractometer with graphite-monochromated Mo-K<sub>α</sub> radiation (λ = 0.71073 Å). Data reduction and absorption correction was performed with HKL Denzo and Scalepack (C1)<sup>[50]</sup> or with SAINT and SADABS (C2 and C3).<sup>[51]</sup> The structure was solved by direct and conventional Fourier methods and all non-hydrogen atoms were refined anisotropically with full-matrix least-squares cycles based on F<sup>2</sup> (XPREDI,<sup>[52]</sup> SHELXS<sup>[53]</sup> and ShelXL<sup>[54]</sup>). Hydrogen atoms were derived from difference Fourier maps and placed at idealised positions, riding on their parent C atoms, with isotropic displacement parameters U<sub>iso</sub>(H) = 1.2U<sub>eq</sub>(C) and 1.5U<sub>eq</sub>(C methyl). All methyl groups were allowed to rotate but not to tip. Data for C4 was collected with a XcaliburS diffractometer from Oxford Diffraction by using the programs CRYVALIS (Oxford, UK, 2008) and CRYVALIS RED (Oxford, UK, 2008) and with graphite-monochromated Mo-K<sub>α</sub> radiation (λ = 0.71073 Å). The structure was solved by direct methods using SHELXS97<sup>[53]</sup> and successive difference Fourier syntheses. For refinement full-matrix least-squares methods were applied (SHELXL97).<sup>[55]</sup> The hydrogen atoms were placed in geometrically calculated positions using a riding model with U<sub>iso</sub> constrained by 1.2 times U<sub>eq</sub> for the carrier atom.

CCDC-1025415 (for C1), CCDC-1025416 (for C2), CCDC-1025417 (for C3) and CCDC-1025418 for (for C4) contain the supplementary crystallographic data for this paper. These data can be obtained free of charge from The Cambridge Crystallographic Data Centre via www.ccdc.cam.ac.uk/data\_request/cif.

**Computational Details:** DFT calculations were performed with the Gaussian 09 program suite.<sup>[41]</sup> The geometries of C1 to C4 and the geometry of the peroxo species were optimised (Table 2) using the nonlocal hybrid meta GGA TPSSH functional<sup>[56]</sup> and the double-ζ basis set 6-31G(d) as implemented in Gaussian on all atoms. The starting geometries for complexes C1 to C4 were generated from the molecular structures. Frequency calculations did not show imaginary values. NBO calculations for the complexes were accomplished by using the NBO 6.0 program suite.<sup>[42–44]</sup> Continuous spectra were plotted with the AOMix program.<sup>[57,58]</sup>

**(2-Quinolinyl)bis(3-*tert*-butylpyrazolyl)methanecopper(I) Chloride [CuCl{HC(3-*t*BuPz)<sub>2</sub>(Qu)}] (C1):** A yellow solution of HC(3-*t*BuPz)<sub>2</sub>(Qu) (0.39 g, 1.00 mmol) dissolved in acetone (5 mL) was added dropwise to a colourless solution of CuCl (0.10 g, 1.00 mmol) dissolved in acetonitrile (20 mL). The solution turned orange and after 18 h a red solid precipitated. After removing the solid matter by filtration, red crystals were obtained from the filtrate at 278 K after several days (0.32 g, 66%). The crystals were characterised by means of X-ray crystallography. IR (ATR):  $\tilde{\nu}$  = 3106 [vw (v, CH<sub>arom</sub>)], 2960 (w), 2904 (vw), 2862 (vw), 1619 (vw), 1596 (w), 1572 (w), 1556 (vw), 1518 (m), 1480 (w), 1456 (w), 1439 (w), 1420 (w), 1392 (vw), 1378 (w), 1363 (w), 1352 (w), 1335 (w), 1307 (vw), 1236 (m), 1186 (vw), 1157 (w), 1124 (vw), 1057 (m), 977 (w), 930 (w), 873 (vw), 842 (w), 827 (w), 806 (m), 790 (m), 775 (vs), 746 (w), 727 (w), 687 (vw), 668 (w), 653 (vw) cm<sup>-1</sup>. MS (FAB+): *m/z* (%) = 487.1 (2) [Cu<sup>37</sup>Cl{HC(3-*t*BuPz)<sub>2</sub>(Qu)}]<sup>+</sup>, 485.1 (2) [Cu<sup>35</sup>Cl{HC(3-*t*BuPz)<sub>2</sub>(Qu)}]<sup>+</sup>, 450.4 (26) [Cu{HC(3-*t*BuPz)<sub>2</sub>(Qu)}]<sup>+</sup>, 388.5 (9) [HC(3-*t*BuPz)<sub>2</sub>(Qu) + H]<sup>+</sup>, 275.1 (7) [HC(Pz)<sub>2</sub>(Qu)]<sup>+</sup>. C<sub>24</sub>H<sub>29</sub>ClCuN<sub>5</sub> (486.52): calcd. C 59.3, H 6.0, N 14.4; found C 59.2, H 6.0, N 14.3.

**(2-Pyridinyl)bis(3-*tert*-butylpyrazolyl)methanecopper(I) Chloride [CuCl{HC(3-*t*BuPz)<sub>2</sub>(Py)}] (C2):** A yellow solution of HC(3-*t*BuPz)<sub>2</sub>(Py) (0.34 g, 1.00 mmol) dissolved in acetone (5 mL) was added dropwise to a colourless solution of CuCl (0.10 g, 1.00 mmol) dissolved in acetonitrile (20 mL). The solution turned yellow and was stored at 278 K overnight, during which time the solution turned light green. Concentration of the solvent until a solid precipitated and storage of the filtrate at 278 K resulted in yellow crystals (0.11 g, 25%). The crystals were characterised by means of X-ray crystallography. IR (ATR):  $\tilde{\nu}$  = 3107 [vw (v, CH<sub>arom</sub>)], 2957 (w), 2904 (w), 2862 (w), 1597 (w), 1574 (vw), 1519 (m), 1478 (w), 1443 (w), 1415 (w), 1392 (vw), 1362 (w), 1348 (w), 1335 (w), 1271 (w), 1236 (m), 1158 (w), 1053 (m), 1013 (w), 1004 (w), 879 (w), 869 (w), 843 (m), 823 (w), 776 (s), 757 (vs), 737 (m), 728 (m), 675 (m), 656 (w) cm<sup>-1</sup>. MS (FAB+): *m/z* (%) = 437.1 (30) [Cu<sup>37</sup>Cl{HC(3-*t*BuPz)<sub>2</sub>(Py)}]<sup>+</sup>, 435.1 (40) [Cu<sup>35</sup>Cl{HC(3-*t*BuPz)<sub>2</sub>(Py)}]<sup>+</sup>, 400.4 (100) [Cu{HC(3-*t*BuPz)<sub>2</sub>(Py)}]<sup>+</sup>. C<sub>20</sub>H<sub>27</sub>ClCuN<sub>5</sub> (436.46): calcd. C 55.0, H 6.2, N 16.1; found C 54.9, H 6.3, N 16.1.

**(2-Pyridinyl)bis(3-*tert*-butylpyrazolyl)methanecopper(II) Bromide [CuBr<sub>2</sub>{HC(3-*t*BuPz)<sub>2</sub>(py)}] (C3):** A yellow solution of HC(3-*t*BuPz)<sub>2</sub>(Py) (0.34 g, 1.00 mmol) dissolved in methanol (5 mL) was added dropwise to a suspension of CuBr<sub>2</sub> (0.22 g, 1.00 mmol) in methanol (7 mL). The mixture was stirred for 20 h. During this time the solution turned dark green and a violet solid precipitated (0.11 g, 19%). Dark red crystals could be obtained by filtration and storage of the filtrate at 278 K for several days. The crystals were characterised by means of X-ray crystallography. IR (ATR):  $\tilde{\nu}$  =

Table 4. Crystallographic data and parameters of C1–C4.

	C1	C2	C3	C4
Empirical formula	C <sub>24</sub> H <sub>29</sub> ClCuN <sub>5</sub>	C <sub>20</sub> H <sub>27</sub> ClCuN <sub>5</sub>	C <sub>20</sub> H <sub>27</sub> Br <sub>2</sub> CuN <sub>5</sub>	C <sub>20</sub> H <sub>27</sub> Cl <sub>2</sub> CuN <sub>5</sub>
Formula mass [g mol <sup>-1</sup> ]	486.51	436.46	560.83	471.91
Crystal size [mm]	0.16 × 0.13 × 0.10	0.18 × 0.17 × 0.11	0.17 × 0.11 × 0.09	0.18 × 0.14 × 0.02
T [K]	200	200	173	173
Crystal system	orthorhombic	monoclinic	monoclinic	orthorhombic
Space group	<i>Pnma</i>	<i>P2<sub>1</sub>/c</i>	<i>P2<sub>1</sub>/c</i>	<i>Pnma</i>
<i>a</i> [Å]	15.017(3)	15.9899(4)	8.0820(6)	15.9418(18)
<i>b</i> [Å]	15.970(3)	16.4751(4)	17.3088(14)	17.563(4)
<i>c</i> [Å]	10.398(2)	16.5686(5)	32.561(2)	8.0627(14)
<i>α</i> [°]	90	90	90	90
<i>β</i> [°]	90	94.82(2)	91.68(2)	90
<i>γ</i> [°]	90	90	90	90
<i>V</i> [Å <sup>3</sup> ]	2493.7(8)	4349.3(2)	4553.0(6)	2257.4(7)
<i>Z</i>	4	8	8	4
<i>ρ</i> <sub>calcd.</sub> [g cm <sup>-3</sup> ]	1.296	1.333	1.636	1.389
<i>μ</i> [mm <sup>-1</sup> ]	1.003	1.141	4.485	1.219
<i>λ</i> [Å]	0.71073	0.71073	0.71073	0.71073
<i>F</i> (000)	1016	1824	2248	980
<i>hkl</i> range	±18, ±19, -11/12	±19, ±19, -19/20	±10, ±21, -36/40	±19, ±21, ±9
Reflections collected	15160	38340	50615	164968
Independent reflections	2403	8081	9286	2175
<i>R</i> <sub>int.</sub>	0.0412	0.0400	0.0327	0.1243
Reflections observed	2403	8081	9286	2175
Number of parameters	163	499	517	142
<i>R</i> <sub>1</sub> [ <i>I</i> ≥ 2σ( <i>I</i> )]	0.0318	0.0358	0.0776	0.0353
<i>wR</i> <sub>2</sub> (all data)	0.0851	0.0916	0.1794	0.0514
Goodness-of-fit	1.083	1.080	1.262	0.649
Largest diff. peak, hole [e Å <sup>-3</sup> ]	-0.302, 0.269	-0.443, 0.479	-0.851, 2.053	-0.255, 0.380

3106 [w (v, CH<sub>arom</sub>)], 3068 [vw (v, CH<sub>arom</sub>)], 2958 (w), 2920 (w), 2868 (vw), 1604 (w), 1522 (m), 1475 (w), 1468 (w), 1447 (m), 1435 (w), 1417 (w), 1393 (vw), 1362 (w), 1343 (w), 1302 (w), 1267 (m), 1236 (s), 1207 (m), 1163 (m), 1111 (w), 1065 (m), 1022 (m), 1000 (w), 928 (vw), 880 (m), 838 (m), 819 (m), 770 (vs), 739 (m), 727 (m), 677 (m), 643 (m), 608 (m) cm<sup>-1</sup>. MS (FAB+): *m/z* (%) = 481.4 (53) [Cu<sup>81</sup>Br{HC(3-*t*BuPz)<sub>2</sub>(Py)}]<sup>+</sup>, 479.4 (47) [Cu<sup>79</sup>Br{HC(3-*t*BuPz)<sub>2</sub>(Py)}]<sup>+</sup>, 400.5 (100) [Cu{HC(3-*t*BuPz)<sub>2</sub>(Py)}]<sup>+</sup>, 338.5 (61) [HC(3-*t*BuPz)<sub>2</sub>(Py)]<sup>+</sup>, 214.4 (98) [HC(3-*t*BuPz)(Py)]. C<sub>20</sub>H<sub>27</sub>Br<sub>2</sub>CuN<sub>5</sub> (560.82): calcd. C 42.8, H 4.9, N 12.5; found C 42.5, H 4.9, N 12.4.

**(2-Pyridinyl)bis(3-*tert*-butylpyrazolyl)methanecopper(II) Chloride [CuCl<sub>2</sub>{HC(3-*t*BuPz)<sub>2</sub>(Py)}] (C4):** A solution of CuCl<sub>2</sub>·2H<sub>2</sub>O (0.17 g, 1.00 mmol) dissolved in methanol (10 mL) was added dropwise to a light yellow solution of HC(3-*t*BuPz)<sub>2</sub>(Py) (0.34 g, 1.00 mmol) dissolved in methanol (6 mL). After several days the formation of green crystals was visible (0.40 g, 85%) IR (KBr):  $\tilde{\nu}$  = 3153 [vw (v, CH<sub>arom</sub>)], 3116 [m (v, CH<sub>arom</sub>)], 3098 [w (v, CH<sub>arom</sub>)], 3068 [w (v, CH<sub>arom</sub>)], 3028 [vw (v, CH<sub>arom</sub>)], 2962 (m), 2907 (w), 2867 (w), 1605 (m), 1576 (vw), 1559 (vw), 1522 (m), 1477 (w), 1450 (m), 1438 (m), 1419 (w), 1391 (vw), 1361 (m), 1351 (m), 1333 (w), 1303 (vw), 1268 (m), 1238 (vs), 1207 (m), 1163 (m), 1110 (vw), 1064 (m), 1022 (m), 1004 (m), 881 (m), 838 (m), 820 (w), 776 (vs), 739 (m), 727 (m), 677 (w), 645 (w), 609 (w), 588 (vw), 520 (vw), 425 (vw) cm<sup>-1</sup>. MS (ESI+, CH<sub>3</sub>OH): *m/z* (%) = 437.1 (4) [Cu<sup>37</sup>Cl{HC(3-*t*BuPz)<sub>2</sub>(Py)}]<sup>+</sup>, 435.1 (8) [Cu<sup>35</sup>Cl{HC(3-*t*BuPz)<sub>2</sub>(Py)}]<sup>+</sup>, 402.2 (10), 401.3 (8), 400.2 (20) [Cu{HC(3-*t*BuPz)<sub>2</sub>(Py)}]<sup>+</sup>, 215.2 (20), 214.2 (100) [HC(3-*t*BuPz)(Py)]<sup>+</sup>. C<sub>20</sub>H<sub>27</sub>N<sub>5</sub>Cl<sub>2</sub>Cu (471.91) calcd. C: 50.9, H: 5.8, N: 14.8; found C 50.6, H: 5.8, N: 14.6.

**Preparation of [Cu{HC(3-*t*BuPz)<sub>2</sub>(Qu)}]SbF<sub>6</sub>:** This complex is the Cu<sup>I</sup> precursor for optical and reactivity studies of the copper dioxygen species. A solution of HC(3-*t*BuPz)<sub>2</sub>(Qu) (0.064 g,

0.17 mmol) in dry CH<sub>2</sub>Cl<sub>2</sub> (2.5 mL) was added in one portion to CuCl (0.017 g; 0.18 mmol). After stirring the mixture for 1 h, a solution of AgSbF<sub>6</sub> (0.062 g, 0.17 mmol) in dry THF (0.25 mL) was added dropwise to the vigorously stirred solution. The resulting slurry, which contained AgCl, was filtered through Celite, thereby resulting in a red-orange solution.

**Preparation of [Cu<sub>2</sub>O<sub>2</sub>{HC(3-*t*BuPz)<sub>2</sub>(Qu)}<sub>2</sub>]SbF<sub>6</sub> (P[SbF<sub>6</sub>]<sub>2</sub>):** Oxygenation of Cu<sup>I</sup> complexes was performed by rapid injection of the 60 mM solution of [Cu{HC(3-*t*BuPz)<sub>2</sub>(Qu)}]SbF<sub>6</sub> (500 μL) into a solution of oxygen in CH<sub>2</sub>Cl<sub>2</sub> (9.5 mL) at 195 K.<sup>[2]</sup> The dichloromethane has been saturated with dioxygen at 195 K for a higher O<sub>2</sub> concentration. In the following, the colour of the solution changed from red-orange to light purple. The formation of P[SbF<sub>6</sub>]<sub>2</sub> was followed by UV/Vis spectroscopy. The pseudo-first-order kinetics (Figure S1) was determined at 195 K and for these measurements we used the same conditions as for the preparation of [Cu{HC(3-*t*BuPz)<sub>2</sub>(Qu)}]SbF<sub>6</sub>.

**Oxidation of Catalytic Amounts of Exogenous Substrate:** This method is analogous to that reported by Tucek et al.<sup>[32]</sup> A solution of 4-methoxyphenol (25 equiv.) and triethylamine (50 equiv.) in dichloromethane (200 μL) was added to the solution of [Cu{HC(3-*t*BuPz)<sub>2</sub>(Qu)}]SbF<sub>6</sub> in CH<sub>2</sub>Cl<sub>2</sub> at 195 K and with a fine needle O<sub>2</sub> was bubbled through this solution. The reaction was monitored by means of UV/Vis spectroscopy. Upon bubbling through O<sub>2</sub>, an intense 418 nm feature developed owing to the formation of the 4-methoxy-1,2-benzoquinone.<sup>[59]</sup> The quantity of the quinone formed was determined from the extinction coefficient of the quinone minus the residual extinction coefficient of thermally decayed P[SbF<sub>6</sub>]<sub>2</sub>, thus yielding ten turnovers per dinuclear copper peroxide species after 1 h.

**Supporting Information** (see footnote on the first page of this article): Selected bond lengths [Å] and angles [°] for both molecules in

the asymmetric unit of C3, the pseudo-first-order plot and DFT-optimised coordinates of C1–C4 and P.

## Acknowledgments

Financial support by the Deutsche Forschungsgemeinschaft (DFG) (DFG-FOR1405 and SFB749-B10) is gratefully acknowledged. Calculation time is gratefully acknowledged from the OCuLUS Cluster at the PC<sup>2</sup> Paderborn and the Leibniz-Rechenzentrum München.

- [1] A. Otero, J. Fernández-Baeza, A. Antiñolo, J. Tejada, A. Lara-Sánchez, *Dalton Trans.* **2004**, 1499–1510.
- [2] A. Hoffmann, C. Citek, S. Binder, A. Goos, M. Rübhausen, O. Troeppner, I. Ivanović-Burmazović, E. C. Wasinger, T. D. P. Stack, S. Herres-Pawlis, *Angew. Chem. Int. Ed.* **2013**, *52*, 5398–5401; *Angew. Chem.* **2013**, *125*, 5508.
- [3] A. Hoffmann, S. Herres-Pawlis, *Chem. Commun.* **2014**, *50*, 403–405.
- [4] S. Trofimenko, J. C. Calabrese, J. S. Thompson, *Inorg. Chem.* **1987**, *26*, 1507–1514.
- [5] M. Rölf, J. Schottenheim, H. Decker, F. Tuczek, *Chem. Soc. Rev.* **2011**, *40*, 4077–4098.
- [6] R. H. Holm, P. Kennepohl, E. I. Solomon, *Chem. Rev.* **1996**, *96*, 2239–2314.
- [7] E. I. Solomon, D. E. Heppner, E. M. Johnston, J. W. Ginsbach, J. Cirera, M. Qayyum, M. T. Kieber-Emmons, C. H. Kjaergaard, R. G. Hadt, L. Tian, *Chem. Rev.* **2014**, *114*, 3659–3853.
- [8] Y. Matoba, T. Kumagai, A. Yamamoto, H. Yoshitsu, M. Sugiyama, *J. Biol. Chem.* **2006**, *281*, 8981–8990.
- [9] J. L. Muñoz-Muñoz, F. García-Molina, R. Varon, P. A. García-Ruiz, J. Tudela, F. García-Cánovas, J. N. Rodríguez-López, *IUBMB Life* **2010**, *62*, 539–547.
- [10] C. Citek, C. T. Lyons, E. C. Wasinger, T. D. P. Stack, *Nat. Chem.* **2012**, *4*, 317–322.
- [11] L. M. Mirica, X. Ottenwaelder, T. D. P. Stack, *Chem. Rev.* **2004**, *104*, 1013–1045.
- [12] N. Kitajima, K. Fujisawa, Y. Moro-oka, K. Toriumi, *J. Am. Chem. Soc.* **1989**, *111*, 8975–8976.
- [13] N. Kitajima, T. Koda, S. Hashimoto, T. Kitagawa, Y. Moro-oka, *J. Am. Chem. Soc.* **1991**, *113*, 5664–5671.
- [14] N. Kitajima, K. Fujisawa, C. Fujimoto, Y. Moro-oka, S. Hashimoto, T. Kitagawa, K. Toriumi, K. Tatum, A. Nakamura, *J. Am. Chem. Soc.* **1992**, *114*, 1277–1291.
- [15] R. Rox Anderson, J. A. Parrish, *J. Invest. Dermatol.* **1981**, *77*, 13–19.
- [16] K. J. McGraw, R. J. Safran, K. Wakamatsu, *Funct. Ecol.* **2005**, *19*, 816–821.
- [17] J. B. Pridham, R. S. Andrews, *Phytochemistry* **1967**, *6*, 13–18.
- [18] R. A. Nicolaus, M. Piattelli, *Rend. Accad. Sci. Fis. Mater.* **1965**, *32*, 83–97.
- [19] K. Fujisawa, T. Ono, Y. Ishikawa, N. Amir, Y. Miyashita, K. Okamoto, N. Lehnert, *Inorg. Chem.* **2006**, *45*, 1698–1713.
- [20] T. D. P. Stack, *Dalton Trans.* **2003**, *34*, 1881–1889.
- [21] T. Osako, K. Ohkubo, M. Taki, Y. Tachi, S. Fukuzumi, S. Itoh, *J. Am. Chem. Soc.* **2003**, *125*, 11027–11033.
- [22] D. J. E. Spencer, A. M. Reynolds, P. L. Holland, B. A. Jazdzewski, C. Duboc-Toia, L. Le Pape, S. Yokota, Y. Tachi, S. Itoh, W. B. Tolman, *Inorg. Chem.* **2002**, *41*, 6307–6321.
- [23] S. Herres-Pawlis, U. Flörke, G. Henkel, *Eur. J. Inorg. Chem.* **2005**, 3815–3824.
- [24] S. Herres-Pawlis, S. Binder, A. Eich, R. Haase, B. Schulz, G. Wellenreuther, G. Henkel, M. Rübhausen, W. Meyer-Klaucke, *Chem. Eur. J.* **2009**, *15*, 8678–8682.
- [25] H.-C. Liang, M. J. Henson, L. Q. Hatcher, M. A. Vance, C. X. Zhang, D. Lahti, S. Kaderli, R. D. Sommer, A. L. Rheingold, A. D. Zuberbühler, E. I. Solomon, K. D. Karlin, *Inorg. Chem.* **2004**, *43*, 4115–4117.
- [26] L. Q. Hatcher, M. A. Vance, A. A. Narducci Sarjeant, E. I. Solomon, K. D. Karlin, *Inorg. Chem.* **2006**, *45*, 3004–3013.
- [27] S. Herres-Pawlis, P. Verma, R. Haase, P. Kang, C. T. Lyons, E. C. Wasinger, U. Flörke, G. Henkel, T. D. P. Stack, *J. Am. Chem. Soc.* **2009**, *131*, 1154–1169.
- [28] L. Q. Hatcher, K. D. Karlin, *Adv. Inorg. Chem.* **2006**, *58*, 131–184.
- [29] D. Petrovic, L. M. R. Hill, P. G. Jones, W. B. Tolman, M. Tamm, *Dalton Trans.* **2008**, 887–894.
- [30] A. Spada, S. Palavicini, E. Monzani, L. Bubacco, L. Casella, *Dalton Trans.* **2009**, 6468–6471.
- [31] M. Réglie, C. Jorand, B. Waegell, *J. Chem. Soc., Chem. Commun.* **1990**, 1752–1755.
- [32] M. Rölf, J. Schottenheim, G. Peters, F. Tuczek, *Angew. Chem. Int. Ed.* **2010**, *49*, 6438–6442; *Angew. Chem.* **2010**, *122*, 6583.
- [33] J. Schottenheim, N. Fateeva, W. Thimm, J. Krahrmer, F. Tuczek, *Z. Anorg. Allg. Chem.* **2013**, *639*, 1491–1497.
- [34] J. N. Hamann, F. Tuczek, *Chem. Commun.* **2014**, *50*, 2298–2300.
- [35] K. V. N. Esguerra, Y. Fall, J.-P. Lumb, *Angew. Chem. Int. Ed.* **2014**, *53*, 5877–5981.
- [36] K. V. N. Esguerra, Y. Fall, L. Petitjean, J.-P. Lumb, *J. Am. Chem. Soc.* **2014**, *136*, 7662–7668.
- [37] A. Hoffmann, U. Flörke, S. Herres-Pawlis, *Eur. J. Inorg. Chem.* **2014**, 2296–2306.
- [38] A. W. Addison, T. Nageswara Rao, J. Reedijk, J. van Rijn, G. C. Verschoor, *J. Chem. Soc., Dalton Trans.* **1984**, 1349–1356.
- [39] L. Yang, D. R. Powell, R. P. Houser, *Dalton Trans.* **2007**, 955–964.
- [40] A. Hoffmann, S. Herres-Pawlis, *Z. Anorg. Allg. Chem.* **2013**, *639*, 1426–1432.
- [41] M. J. Frisch, G. W. Trucks, H. B. Schlegel, G. E. Scuseria, M. A. Robb, J. R. Cheeseman, G. Scalmani, V. Barone, B. Mennucci, G. A. Petersson, H. Nakatsuji, M. Caricato, X. Li, H. P. Hratchian, A. F. Izmaylov, J. Bloino, G. Zheng, J. L. Sonnenberg, M. Hada, M. Ehara, K. Toyota, R. Fukuda, J. Hasegawa, M. Ishida, T. Nakajima, Y. Honda, O. Kitao, H. Nakai, T. Vreven, J. A. Montgomery Jr., J. E. Peralta, F. Ogliaro, M. Bearpark, J. J. Heyd, E. Brothers, K. N. Kudin, V. N. Staroverov, R. Kobayashi, J. Normand, K. Raghavachari, A. Rendell, J. C. Burant, S. S. Iyengar, J. Tomasi, M. Cossi, N. Rega, J. M. Millam, M. Klene, J. E. Knox, J. B. Cross, V. Bakken, C. Adamo, J. Jaramillo, R. Gomperts, R. E. Stratmann, O. Yazyev, A. J. Austin, R. Cammi, C. Pomelli, J. W. Ochterski, R. L. Martin, K. Morokuma, V. G. Zakrzewski, G. A. Voth, P. Salvador, J. J. Dannenberg, S. Dapprich, A. D. Daniels, O. Farkas, J. B. Foresman, J. V. Ortiz, J. Cioslowski, D. J. Fox, *Gaussian 09*, revision B.01, Gaussian, Inc., Wallingford CT, **2010**.
- [42] F. Weinhold, C. Landis, *Valency and Bonding - A Natural Bond Orbital Donor-Acceptor Perspective*, Cambridge University Press, New York, **2005**.
- [43] E. D. Glendening, C. R. Landis, F. Weinhold, *J. Comput. Chem.* **2013**, *34*, 1429–1437.
- [44] E. D. Glendening, J. K. Badenhoop, A. E. Reed, J. E. Carpenter, J. A. Bohmann, C. M. Morales, C. R. Landis, F. Weinhold, *NBO 6.0*, Theoretical Chemistry Institute, University of Wisconsin, Madison, **2013**.
- [45] R. S. Himmelwright, N. C. Eickman, C. D. LuBien, K. Lerch, E. I. Solomon, *J. Am. Chem. Soc.* **1980**, *102*, 7339–7344.
- [46] R. L. Martin, *J. Chem. Phys.* **2003**, *118*, 4775–4777.
- [47] J. Leonhard, B. Lygo, G. Procter, *Praxis in der Organischen Chemie*, VCH Verlagsgesellschaft, Weinheim, Germany, **1996**.
- [48] A. Hoffmann, U. Flörke, M. Schürmann, S. Herres-Pawlis, *Eur. J. Org. Chem.* **2010**, 4136–4144.
- [49] H.-D. Hardt, *Z. Anorg. Allg. Chem.* **1959**, *301*, 87–96.
- [50] Z. Otwinowski, W. Minor, in: *Int. Tables Crystallogr.* vol. F (Ed.: M. G. Rossmann), Kluwer Academic Publishers, Dordrecht/Boston/London, **2001**, p. 226–235.

- [51] Bruker, SMART (version 5.62), SAINT (version 6.02), SHELXTL (version 6.10), SADABS (version 2.03), AXS Inc., Madison, Wisconsin, USA, **2002**.
- [52] Bruker, *XPREP*, Bruker AXS Inc., Madison, Wisconsin, USA, **2007**.
- [53] G. M. Sheldrick, *Acta Crystallogr., Sect. A* **1990**, *46*, 467–473.
- [54] C. B. Hübschle, G. M. Sheldrick, B. Dittrich, *J. Appl. Crystallogr.* **2011**, *44*, 1281–1284.
- [55] G. M. Sheldrick, *SHELXL*, University of Göttingen, Germany, **1997**.
- [56] J. Tao, J. P. Perdew, V. N. Staroverov, G. E. Scuseria, *Phys. Rev. Lett.* **2003**, *91*, 146401-1-146401-4.
- [57] S. I. Gorelsky, *AOMix: Program for Molecular Orbital Analysis*, <http://www.sg-chem.net/>, **1997**.
- [58] S. I. Gorelsky, S. Ghosh, E. I. Solomon, *J. Am. Chem. Soc.* **2006**, *128*, 278–290.
- [59] S. I. Bailey, I. M. Ritchie, Z. Hong-Guang, *Bioelectrochem. Bioenerg.* **1988**, *19*, 521–531.

Received: October 7, 2014

Published Online: ■

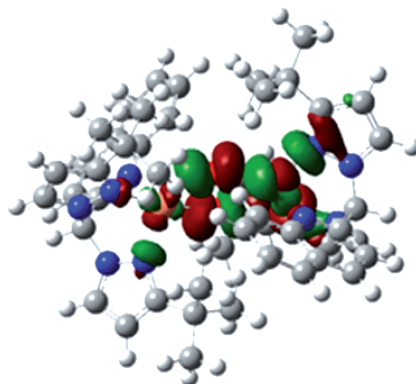
## Bioinorganic Chemistry

C. Wilfer, P. Liebhäuser, H. Erdmann,  
A. Hoffmann, S. Herres-Pawlis\* ..... 1–10



Biomimetic Hydroxylation Catalysis  
Through Self-Assembly of a Bis(pyrazolyl)-  
methane Copper–Peroxo Complex

**Keywords:** Bioinorganic chemistry / Oxygen  
activation / Self-assembly / Copper / N  
ligands



Herein, we present four new bis(pyrazolyl)-methane–copper complexes. Furthermore, we studied the self-assembly of a peroxo–dicopper species with catalytic hydroxylation activity of phenols by UV/Vis spectroscopy. The donor competition between pyrazolyl and pyridinyl units as well as the UV transitions of the tyrosinase model have been investigated by density functional theory.